13th World Conference on Earthquake Engineering
Vancouver, B.C., Canada
August 1-6, 2004
Paper No. 2090

AN ANALYTICAL SIMULATION OF THE SEISMIC FIELD IN A SLOPING ALLUVIAL LAYER OVER A ROCK BASEMENT

Piotr BOREJKO[1]

SUMMARY

An analytical simulation of the seismic field is presented for a wedge-shaped alluvial layer overlying a rock basement (a dipping structure). Time domain responses, illustrating essential features of seismic propagation in a three-dimensional (3-D) alluvial wedge, are evaluated at receivers located down-dip, cross-slope, and up-dip of a point source located within the wedge. This simulation of the field is adequate in that it accounts for seismic penetration of the bottom characteristic for a real rock, but it is intrinsically unable to include contributions from the *S*-phases of the field typically present in a real alluvial ground.

1. INTRODUCTION

One of the important factors in the aseismic (earthquake resistant) design of structures is the surface layer magnification of earthquake motion (Okamoto [1]). In alluvial ground, where the magnification is pronounced, seismic intensity maps showing the predominant frequency and the magnification factor at each zone have been prepared (e.g., Tokyo metropolitan area) for use in aseismic design. Theoretically, both frequencies and magnification factors are calculated on the basis of horizontally layered model for the ground, the thickness of each layer being assumed uniform. The non-uniformity of layers can significantly change the response of the medium. Seismic damage of surface structures over a small area often varies considerably from one cross section of the ground to another (Poceski [2], and Murphy and Hewlett [3]). One reason for such a variation is the change of local geological and soil structure, particularly the inclination of a layer to ground surface known as a dipping structure.

In this article, we present a time domain analytical solution, derived by applying the ray-integral method (Pao and Gajewski [4], and Borejko and Ziegler [5]), for the seismic wave-field due to a point source in an alluvial wedge with a rock basement. In evaluating this solution no approximations are introduced into the mathematical formulation of the problem and integral representations for partial waves contributing to the response are exact, so that the solution is valid for all receiver-locations. Besides the seismic response, the solution also evaluates the travel times and the propagation paths for partial waves contributing to the response.

[1] Docent, Institute of Rational Mechanics, Department of Civil Engineering, Vienna University of Technology, A–1040 Vienna, Austria, Email: pb@allmech.tuwien.ac.at

2. FORMULATION OF THE PROBLEM

The geometry for the present dipping-structure problem is shown in Fig. 2.1. A wedge-shaped alluvial layer (an alluvial wedge), bounded above by a horizontal planar surface (ground surface) and below by a dipping (sloping, inclined downward) planar interface, overlies a substratum (a rock basement). The boundary planes of this non-uniform surface layer intersect along the line of apex and the apex angle (the wedge angle) α is measured through the interior of the layer. A seismic point source is located within the layer, and the layer thickness (measured vertically) at the source-location is h.

The alluvial ground composing the layer is homogeneous and water-saturated, the state of stress at any point in the layer is then assumed to be given by $\boldsymbol{\sigma} = -p\mathbf{I}$, and such an alluvial ground can thus be characterized by the mass density ρ and the P wave speed c. The fast-speed substratum is assumed to be a homogeneous solid elastic medium of mass density ρ_2 and of P and S wave speeds c_p and c_s, respectively, where $c_p > c_s > c$.

The task is to derive and analyze the solution for the 3-D seismic field due to the point source at any receiver located within this non-parallel layer.

In the analysis, we use two Cartesian coordinate systems (x,y,z) and (x',y',z'), and the common origin 0 of the two coordinate systems is located at the horizontal boundary plane of the wedge (at the distance d from the apex line) directly above the point source, so that $d = h\cos\alpha/\sin\alpha$. The x, y, and z are the range (normal to the apex), the cross-range (parallel to the apex), and the depth coordinate axes, respectively. The y' axis is congruent with the y axis, and the x' and z' axes are obtained by rotating the x and z axes, respectively, through the angle α about the y axis, so that the x' axis is parallel to the dipping boundary plane of the wedge and the z' axis is normal to this plane. The point source is then located in the plane $y = 0$ (the main vertical plane) at a depth z_0 directly below the origin 0.

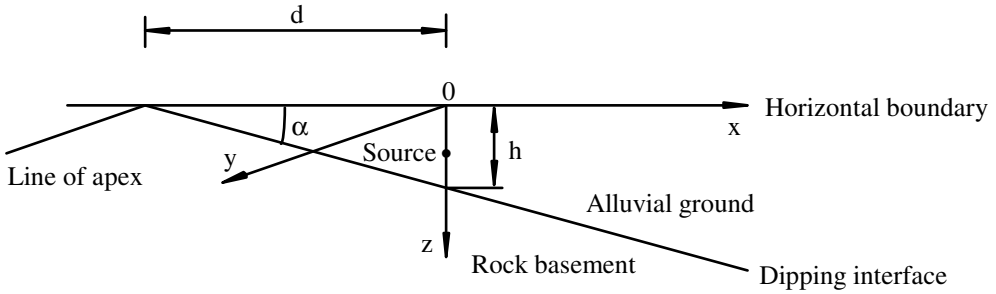

Fig. 2.1. The geometry for a wedge-shaped alluvial layer overlying a rock basement.

2.1. The Governing Equations

In a water-saturated alluvial wedge, the 3-D wave-field can be specified by the velocity potential function ϕ that satisfies the quiescent initial conditions $\phi = 0$ and $\partial\phi/\partial t = 0$ at $t = 0$, and the three-dimensional inhomogeneous wave equation

$$c^2\nabla^2\phi - \frac{\partial^2\phi}{\partial t^2} = -f(t)\delta(x)\delta(y)\delta(z - z_0),$$

where the causal function $f(t)$ (i.e., $f(t)=0$ for $t<0$) specifies the time history of ϕ at the source. The pressure p and the velocity $\mathbf{v}$ are $p=-\rho\partial\phi/\partial t$ and $\mathbf{v}=\nabla\phi$, respectively.

In a solid substratum, the 3-D wave-field is characterized by the displacement vector $\mathbf{u}$ that satisfies the Navier-Cauchy equation of motion, and the stress $\boldsymbol{\sigma}$ is related to the displacement gradient $\nabla\mathbf{u}$ by Hooke's law for isotropic elastic medium.

2.2. The Boundary Conditions

The horizontal boundary $z=0$ is free (i.e., the boundary $z=0$ is a perfect reflector), so that the boundary condition for p is

$$p=0 \quad \text{at} \quad z=0,$$

and the reflection coefficient for plane waves $R_{(1)}^{PP}$ is thus constant at $z=0$:

$$R_{(1)}^{PP}=-1.$$

At the dipping boundary $z'=h\cos\alpha$ separating a water-saturated alluvial ground from a rock basement, the boundary conditions (with reference to the primed coordinate system) are

$$p=-\sigma'_{zz}, \quad v'_z=\frac{\partial u'_z}{\partial t}, \quad \sigma'_{zx}=0, \quad \sigma'_{zy}=0,$$

and the reflection coefficient for plane waves $R_{(2)}^{PP}$ at $z'=h\cos\alpha$ is

$$R_{(2)}^{PP}=\frac{\rho_2 c_s^4\,\zeta'_0 H(\xi'_0,\eta'_0)-\rho\sqrt{c_p^{-2}+\xi'^2_0+\eta'^2_0}}{\rho_2 c_s^4\,\zeta'_0 H(\xi'_0,\eta'_0)+\rho\sqrt{c_p^{-2}+\xi'^2_0+\eta'^2_0}},$$

where ξ'_0, η'_0, $\zeta'_0=\sqrt{c^{-2}+\xi'^2_0+\eta'^2_0}$ are the wave slownesses and $H(\xi'_0,\eta'_0)$ is the Rayleigh function:

$$H(\xi'_0,\eta'_0)=[2(\xi'^2_0+\eta'^2_0)+c_s^{-2}]^2-4(\xi'^2_0+\eta'^2_0)\sqrt{c_p^{-2}+\xi'^2_0+\eta'^2_0}\sqrt{c_s^{-2}+\xi'^2_0+\eta'^2_0}.$$

3. THE SEISMIC FIELD IN A WATER-SATURATED ALLUVIAL WEDGE

In a water-saturated alluvial wedge, the seismic field produced by a point source consists of two components: the diffraction field due to scattering at the apex and the image field given by a sum of partial waves, where the 0-th order wave is that radiated from the source and the k-th order wave ($k=1,2,3,...$) is that reflected k-times off the wedge boundaries before arriving at the receiver.

3.1. The Analytical Solution for the Seismic Field

The diffraction field is ignored entirely in the following discussion, and the 3-D seismic field is thus given by the image field, expressed by a sum of partial waves

$$\phi=\phi_0+\phi_{\pm1}+\phi_{\pm2}+\phi_{\pm3}+\cdots,$$

where ϕ_0 is the wave radiated from the source and $\phi_{\pm k}$ $(k=1,2,3,...)$ is the multi-reflected wave undergoing reflections from the horizontal boundary $z=0$ and the dipping boundary $z'=h\cos\alpha$. In $\phi_{\pm k}$, the k letter indicates the number of reflections from the boundaries, the $+$ sign indicates that the first reflection is from the dipping boundary $z'=h\cos\alpha$, and the $-$ sign indicates that the first reflection is from the horizontal boundary $z=0$, so that ϕ_{+k} is the $+k$-th partial wave that undergoes k consecutive reflections from the boundaries, the first reflection being from the dipping boundary $z'=h\cos\alpha$, and ϕ_{-k} is the $-k$-th partial wave that undergoes k consecutive reflections from the boundaries, but the first reflection being now from the horizontal boundary $z=0$.

The solution for ϕ_0 is represented by the spherical P wave of the form

$$\phi_0 = f(t-R/c)/4\pi c^2 R,$$

where $R^2 = x^2+y^2+(z-z_0)^2$ and R is the distance from the source-point $\boldsymbol{x}_0$ to the receiver-point $\boldsymbol{x}$. Since $p_0 = -\rho\partial\phi_0/\partial t$, the pulse p_0 due to the 0-th wave (the seismic pulse emitted by the source) is

$$p_0(t) = (p_c/R)\frac{\partial}{\partial t}\left[f(t-R/c)\right], \tag{3.1}$$

where $p_c = -\rho/4\pi c^2$, and the pulse p_0 is decaying as R^{-1}.

The solution for $\phi_{\pm k}$ is derived by applying the ray-integral method. This (in the first instance Laplace-transformed) solution appears as a double integral over an infinite domain (so-called ray integral) that is synthesized by superposition of plane wave components whose amplitudes are cumulative products of the reflection coefficients and whose phase functions are derived by applying the method of images. This ray integral is then transformed into the time domain by applying the Cagniard-de Hoop method where it emerges as a single definite integral

$$I_{\pm k}(t) = \frac{1}{2\pi^2 c^2} H(t-t_A)\,\mathrm{Re}\int_0^{q(t)} S\,\Pi_{\pm k}\,\frac{dg_{\pm k}^{-1}}{dt}\,dq$$

taken (at specific observation time t) over a fixed finite interval $[0,q(t)]$ in the wave slowness q. In the above, t_A is the (respective) minimum arrival time of the $\pm k$-th wave, $H(t)$ is the Heaviside step function, Re denotes the real part, S is the source function, $\Pi_{\pm k}$ is the cumulative product of consecutive reflection coefficients, and $g_{\pm k}^{-1}$ is the inverse of the phase function $g_{\pm k}$. The ray integral $I_{\pm k}(t)$ is further transformed into a form amenable to numerical integration accomplished by the Gaussian quadrature. The values of $I_{\pm k}(t)$ (computed at a preselected time interval) are convoluted with the time function (the time signature) of the source to obtain the (complete) partial seismic response $p_{\pm k}$ due to the $\pm k$-th wave:

$$p_{\pm k}(t) = -\rho\int_{t_A}^{t}\frac{\partial^2}{\partial t^2}\left[f(t-\tau)\right]I_{\pm k}(\tau)\,d\tau\,.$$

This partial response includes the contribution from the multi-reflected spherical P wave and (depending on the receiver position relative to the source, the number of consecutive reflections, and the geo-seismic parameters of alluvial ground and rock basement) a number of contributions from the head waves

(critically refracted waves) and the pseudo-Rayleigh and Stoneley interface waves. Note that in evaluating this response no approximation is introduced. Besides the solution for $p_{\pm k}$, the ray-integral method also computes the minimum arrival times and the propagation paths for the multi-reflected spherical and head P waves in the wedge.

When the apex angle α is an integer submultiple of π ($N\alpha = \pi$, where N is an integer), the solution for the seismic field p (the seismic response p due to the image field component) at the receiver-point $\boldsymbol{x}$ is

$$p = p_0 + \sum_{k=1}^{N} p_{+k} + \sum_{k=1}^{N} p_{-k} \,. \tag{3.2}$$

3.2. The Propagation Paths

The $\pm k$-th spherical P wave propagates in the wedge along the $\pm k$-th ray path (the $\pm k$-th stationary time path) connecting the source-point $\boldsymbol{x}_0$ with the receiver-point $\boldsymbol{x}$ via successive reflection-points. This $\pm k$-th ray path, constructed geometrically by the method of images, can be identified as a fictitious straight ray (of length $R_{\pm k}$) from one image of the source-point $\boldsymbol{x}_0$ to one image of the receiver-point $\boldsymbol{x}$.

The head P wave (with conical wave front) and the pseudo-Rayleigh and Stoneley interface waves are generated in the wedge when the angle of incidence of the spherical P wave (that is incident from the wedge upon the fast-speed substratum) exceeds the critical angle, i.e., when the spherical P wave is totally reflected from the fast-speed substratum. Specifically, when $c_p > c_s > c$, two head P waves are generated in the wedge provided that $\gamma > \gamma_{cs} > \gamma_{cp}$, where γ is the angle of incidence, and $\gamma_{cs} = \sin^{-1}(c/c_s)$ and $\gamma_{cp} = \sin^{-1}(c/c_p)$ are the critical angles. The head wave fronts propagating along the refracted ray paths arrive at the receiver ahead of those following the stationary time paths. The refracted ray paths in the wedge can also be constructed geometrically by the method of images.

In the wedge, the local angle of incidence of the $\pm k$-th spherical P wave changes from one reflection to the next. On successive reflections from either one of the wedge boundaries, this angle decreases by twice the apex angle for the up-dip propagation and increases by twice the apex angle for the down-dip propagation. The $\pm k$-th spherical P wave may thus strike the bottom either at steep angles (smaller than the critical angles γ_{cs} and γ_{cp}), where partial reflection occurs with seismic energy loss into the bottom, or at shallow angles (greater than the critical angles γ_{cs} and γ_{cp}), where total reflection occurs with no energy loss. The head P waves are generated by these bottom reflections, where the local angle of incidence exceeds the critical angles γ_{cs} and γ_{cp}.

The multiple interactions of the $\pm k$-th spherical P wave with the fast-speed bottom may thus initiate a great number of the head P waves (arriving at the receiver-point $\boldsymbol{x}$ ahead of the $\pm k$-th spherical P wave) and a great number of the pseudo-Rayleigh and Stoneley interface waves propagating in the wedge along the dipping interface $z' = h\cos\alpha$. The head P wave that arrives first at the receiver-point $\boldsymbol{x}$ (the $\pm k$-th primary head P wave) is always initiated either by the first bottom reflection or the ultimate bottom reflection of the $\pm k$-th spherical P wave. The head P waves that follow the $\pm k$-th primary head P wave are referred to as the secondary head P waves.

Since the wedge is a nonparallel-sided wave guide, the stationary time paths and the refracted ray paths are essentially three-dimensional. When the receiver-point $\boldsymbol{x}$ is located out of the main vertical plane

$y=0$ containing the source-point $\boldsymbol{x}_0$, the repeated reflections at the dipping boundary $z'=h\cos\alpha$ introduce the curvature into the projection of the respective path onto the horizontal boundary $z=0$, because the local plane of incidence is not a vertical plane for each bottom reflection. This path curvature in the horizontal plane is known as "horizontal refraction". Note that the whole path is in the main vertical plane $y=0$ (i.e., the path is two-dimensional) when the receiver-point $\boldsymbol{x}$ is also in this plane.

When the first reflection point is located up-dip from the source, then, in the course of successive up-dip reflections, the local angle of incidence may become so small that the path is turned around and the wave front (the spherical P wave front or the head P wave front) proceeds to travel down-dip. This change in propagation direction is known as "backscattering". Depending on the number of consecutive reflections k, the respective wave fronts thus reach the receiver-point $\boldsymbol{x}$ along one of the two paths: the direct path or the indirect path (the backscattered path) which is turned around on approaching the apex of the wedge.

4. THE CALCULATION OF THEORETICAL SEISMOGRAMS

In this section, we examine the effect of the receiver-location on theoretical seismograms (time records of the seismic response) when the receivers are located in the wedge at equal radial range in the horizontal plane from the source-point $\boldsymbol{x}_0$, but different orientation relative to the source-point $\boldsymbol{x}_0$. The apex angle α is set at $\alpha=10^{\circ}$, so that in (3.2) $N=18$, and 37 partial waves contribute to the seismic response.

For the convenience of numerical calculations, all quantities having the dimension of length are normalized by h, the wedge thickness at the source-location, all quantities having the dimension of time are normalized by the characteristic time t_c (defined by $t_c = h/c$), and each partial seismic response (p_0 and $p_{\pm k}$) is normalized by p_c.

4.1. The Geo-Seismic Parameters and the Source-Pulse

The geo-seismic parameters assumed for a water-saturated alluvial wedge are $c=1$ and $\rho=1$, and the wedge thickness at the source-location is $h=1$. The properties assumed for a rock basement are $c_p=\sqrt{3}c_s$, $c_s=2.19$, and $\rho_2=2.5$. We thus consider the fast-speed substratum with discontinuities at the dipping interface $z'=h\cos\alpha$ both in the propagation speeds and in the mass density. The critical angles for the substratum are $\gamma_{cs}=27.17^{\circ}$ and $\gamma_{cp}=15.29^{\circ}$.

For the numerical calculations of the theoretical seismograms, we assume that the source-pulse p_0 [eq. (3.1)] has the shape of an isosceles triangle, where Δ is the rise time of the pulse, 2Δ is the pulse duration, and $(p_c/R)\Delta$ is the peak value of the pulse. When $\Delta\to 0$, the pulse adopts the shape of the Dirac delta function. For instance, when $R/h=4$ and $\Delta/t_c=0.05$, the response p_0/p_c due to this triangular source-pulse sets up at time $t/t_c=4$, has the shape of an isosceles triangle, the response duration is $2\Delta/t_c=0.1$, and the peak value of the response is 0.0125 at time $t/t_c=4.05$.

4.2. Results

The source and each and every receiver are located on the bisecting plane of the wedge (the bisector of the wedge). The source depth is $z_0=d\tan(\alpha/2)$, so that the normalized range of the source from the apex line is $d/h=\cot 10^{\circ}$ and the normalized source depth is $z_0/h=\cot 10^{\circ}\tan 5^{\circ}$ for a 10° wedge. The x, y, and z coordinates of each and every receiver are, respectively, $x=r\cos\gamma$, $y=r\sin\gamma$, and

$z = (d + r\cos\gamma)\tan(\alpha/2)$, where r is the radial range in the horizontal plane $z = 0$ (shortly, the radial range) and γ is the azimuth angle measured clockwise in this plane from the x axis.

To examine the effect of the receiver-location on the seismic response in the wedge, we select three receivers having the same radial range r, but different azimuth angle γ. For a 10^o wedge, we thus assume $\gamma = 0^o$, 90^o, 180^o and $r = 5h$, and the three receiver-locations are

$$\begin{aligned} \boldsymbol{x}_1 &= [5, 0, (\cot 10^o + 5)\tan 5^o], && (\gamma_1 = 0^o), \\ \boldsymbol{x}_2 &= (0, 5, \cot 10^o \tan 5^o), && (\gamma_2 = 90^o), \\ \boldsymbol{x}_3 &= [-5, 0, (\cot 10^o - 5)\tan 5^o], && (\gamma_3 = 180^o), \end{aligned} \tag{4.1}$$

where the components of $\boldsymbol{x}_1$, $\boldsymbol{x}_2$, and $\boldsymbol{x}_3$ are normalized by h. Relative to the source-point $\boldsymbol{x}_0$, $\boldsymbol{x}_1$ is the down-dip position, $\boldsymbol{x}_2$ is the cross-slope position, and $\boldsymbol{x}_3$ is the up-dip position.

The theoretical seismograms were evaluated at three locations [eqs. (4.1)], as is shown in Fig. 4.1 for the triangular source-pulse p_0 of $\Delta/t_c = 0.05$, where the normalized seismic response p/p_c is plotted against the normalized time t/t_c.

At each receiver, the partial waves are arranged in ascending order according to their minimum arrival times, as is shown in Tables A.1, A.2, and A.3. In these tables, $\tau_{\pm lp} = t_{\pm lp}/t_c$, $\tau_{\pm ls} = t_{\pm ls}/t_c$, and $\tau_M = t_M/t_c$, where $t_{\pm lp}$, $t_{\pm ls}$, and t_M are the arrival times of the faster primary head P wave, the slower primary head P wave, and the spherical P wave, respectively. (The minimum arrival times of the secondary head P waves and the pseudo-Rayleigh and Stoneley interface waves are not shown in these tables.) Since the source and the receivers are located on the bisector of the wedge, the lengths of the $+k$-th and $-k$-th ray paths are identical, so that the $+k$-th and $-k$-th spherical P waves arrive simultaneously. In these tables, the superscript appended to a value of the particular arrival time specifies the propagation path: The (d) superscript means that the wave arrives at the receiver along the direct path, and the (i) superscript means that the wave arrives at the receiver along the indirect path which is turned around on approaching the apex of the wedge.

All spherical P waves interacting with the sloping bottom $z' = h\cos\alpha$ undergo at least one total reflection off the bottom (Tables A.1, A.2, and A.3), and, at each of the three locations, the source-pulse (indicated in Fig. 4.1 by the vertical arrow) is preceded by a number of the (primary and secondary) head P waves and the seismic response begins with the arrival of the $+1$-st (faster) primary head P wave.

The two critical angles for the fast-speed substratum are steep ($\gamma_{cs} = 27.17^o$ and $\gamma_{cp} = 15.29^o$). Hence, the penetration of the seismic energy into the bottom is weak, and thus even the later arriving partial waves make significant contributions to the seismic responses (Fig. 4.1). As the azimuth angle γ increases, the duration of the phase preceding the source-pulse also increases, but the duration of the phase following the source-pulse decreases, and the pulses following the source-pulse become more peaked.

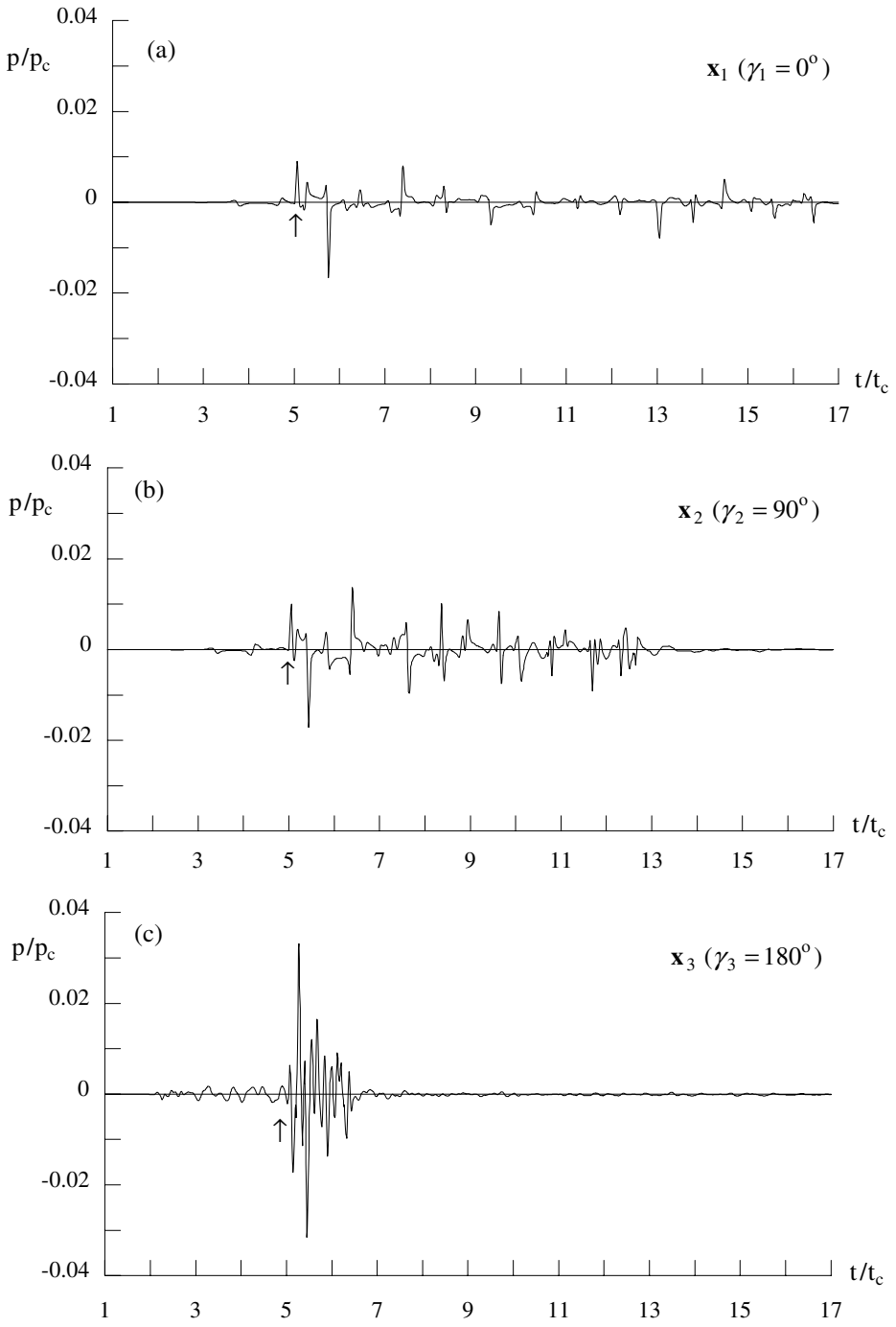

Fig. 4.1. The seismic response in a sloping water-saturated alluvial layer $(c=1,\ \rho=1)$ with a fast-speed rock basement $(c_p=\sqrt{3}c_s,\ c_s=2.19,\ \rho_2=2.5)$ due to a buried point source emitting the triangular pulse; (a) at location $\boldsymbol{x}_1$ $(\gamma_1=0^{\circ})$; (b) at location $\boldsymbol{x}_2$ $(\gamma_2=90^{\circ})$; (c) at location $\boldsymbol{x}_3$ $(\gamma_3=180^{\circ})$. The source is located in the sloping layer at $\boldsymbol{x}_0=(0,0,\cot 10^{\circ}\tan 5^{\circ})$, and the vertical arrow indicates the arrival time of the source-pulse.

5. CONCLUSIONS

The purpose of this article was to present an analytical solution for the seismic field in an alluvial wedge overlying a rock basement. The contribution from the diffracted field is not included in the solution, nevertheless the solution is exact and complete for the image field because no approximations were introduced into the mathematical formulation of this dipping-structure problem, and the ray integrals representing partial waves are exact. The solution is adequate in that it accounts for seismic penetration of the bottom characteristic for a real rock, but it is intrinsically unable to include contributions from the *S*-phases of the field typically present in a real alluvial ground.

The point source and three receivers were placed on the bisecting plane of the wedge, each receiver had the same radial range in the horizontal from the source, but different orientation to the source, measured by the azimuth angle assuming values 0^o (down-dip), 90^o (cross-slope), and 180^o (up-dip). Time records of the seismic response due to the complete image field were evaluated at the three receivers for a triangular source-pulse. The arrival times of the spherical and head waves along various (direct and backscattered) paths at the three receivers were also given.

The time records of the seismic response and the arrival times provided information about the 3-D seismic field in the wedge. The time interval between the first arrival and the ultimate arrival diminished, and the pulses following the source-pulse became more peaked, as the azimuth angle of the receiver increased. The two critical angles for the fast-speed rock basement were steep, so that the penetration of the seismic energy into the substratum was weak, and the backscattered pulses made significant contributions to these records.

6. REFERENCES

1. Okamoto S. “Introduction to earthquake engineering.” New York: John Wiley, 1971.
2. Poceski A. “The ground effects of the Skopje July 26, 1963 earthquake.” Bull. Seism. Soc. Am. 1969; 59: 1-22.
3. Murphy JR, Hewlett RA “Analysis of seismic response in the City of Las Vegas, Nevada: a preliminary microzonation.” Bull. Seism. Soc. Am. 1975; 65: 1575-1597.
4. Pao YH, Gajewski RR “The generalized ray theory and transient responses of layered elastic solids.” Physical Acoustics 1977; 13: 184-265.
5. Borejko P, Ziegler F “Pulsed asymmetric point force loading of a layered half-space.” Guran A, Boström A, Leroy O, Maze G, Editors. Acoustic interactions with submerged elastic structures. Singapore: World Scientific, 2002: 307-388.

APPENDIX A

Table A.1. Arrival times for the partial waves in a sloping water-saturated alluvial layer with a fast-speed rock basement [at location $\boldsymbol{x}_1$ ($\gamma_1 = 0^{\circ}$)].

Partial wave	$\tau_{\pm lp}$	$\tau_{\pm ls}$	τ_M
ϕ_{+1}	$2.6952^{(d)}$	$3.5551^{(d)}$	$5.2004^{(d)}$
ϕ_{-2}	$3.6834^{(d)}$	$4.5033^{(d)}$	$5.7050^{(d)}$
ϕ_{+2}	$4.3839^{(d)}$	$5.0430^{(d)}$	$5.7050^{(d)}$
ϕ_{+3}	$4.6723^{(i)}$	$5.4878^{(d)}$	$6.4445^{(d)}$
ϕ_{0}			$5.0191^{(d)}$
ϕ_{-1}			$5.2004^{(d)}$
ϕ_{-3}	$5.3721^{(d)}$	$5.9912^{(d)}$	$6.4445^{(d)}$
ϕ_{-4}	$5.6320^{(i)}$	$6.4790^{(i)}$	$7.3298^{(d)}$
ϕ_{+18}	$5.6801^{(i)}$	$8.7344^{(i)}$	$16.4050^{(i)}$
ϕ_{-18}	$5.6801^{(i)}$	$8.7344^{(i)}$	$16.4050^{(i)}$
ϕ_{+4}	$6.3610^{(i)}$	$6.9757^{(d)}$	$7.3298^{(d)}$
ϕ_{+5}	$6.5332^{(i)}$	$7.4465^{(i)}$	$8.2921^{(d)}$
ϕ_{+17}	$6.5776^{(i)}$	$9.5252^{(i)}$	$16.3484^{(i)}$
ϕ_{-5}	$7.3207^{(i)}$	$7.9669^{(i)}$	$8.2921^{(d)}$
ϕ_{-6}	$7.3487^{(i)}$	$8.3612^{(i)}$	$9.2831^{(d)}$
ϕ_{-16}	$7.3879^{(i)}$	$10.1998^{(i)}$	$16.1793^{(i)}$
ϕ_{+7}	$8.0535^{(i)}$	$9.1950^{(i)}$	$10.2685^{(i)}$
ϕ_{+15}	$8.0864^{(i)}$	$10.7378^{(i)}$	$15.8992^{(i)}$
ϕ_{+6}	$8.2219^{(i)}$	$8.9344^{(i)}$	$9.2830^{(d)}$
ϕ_{-8}	$8.6264^{(i)}$	$9.9228^{(i)}$	$11.2240^{(i)}$
ϕ_{-14}	$8.6519^{(i)}$	$11.1228^{(i)}$	$15.5109^{(i)}$
ϕ_{+16}	$8.8935^{(i)}$	$11.4917^{(i)}$	$16.1792^{(i)}$
ϕ_{-7}	$9.0374^{(i)}$	$9.8491^{(i)}$	$10.2685^{(i)}$
ϕ_{+9}	$9.0498^{(i)}$	$10.5223^{(i)}$	$12.1308^{(i)}$
ϕ_{+13}	$9.0673^{(i)}$	$11.3432^{(i)}$	$15.0185^{(i)}$
ϕ_{-17}	$9.0765^{(i)}$	$11.6877^{(i)}$	$16.3484^{(i)}$
ϕ_{-10}	$9.3109^{(i)}$	$10.9754^{(i)}$	$12.9745^{(i)}$
ϕ_{-12}	$9.3198^{(i)}$	$11.3922^{(i)}$	$14.4271^{(i)}$
ϕ_{+11}	$9.4018^{(i)}$	$11.2684^{(i)}$	$13.7431^{(i)}$
ϕ_{+8}	$9.7422^{(i)}$	$10.6829^{(i)}$	$11.2240^{(i)}$
ϕ_{-9}	$10.3151^{(i)}$	$11.4107^{(i)}$	$12.1309^{(i)}$
ϕ_{-15}	$10.3406^{(i)}$	$12.6107^{(i)}$	$15.8992^{(i)}$
ϕ_{+10}	$10.7385^{(i)}$	$12.0102^{(i)}$	$12.9744^{(i)}$
ϕ_{+14}	$10.7560^{(i)}$	$12.8311^{(i)}$	$15.5109^{(i)}$
ϕ_{-11}	$10.9996^{(i)}$	$12.4633^{(i)}$	$13.7431^{(i)}$
ϕ_{-13}	$11.0085^{(i)}$	$12.8801^{(i)}$	$15.0185^{(i)}$
ϕ_{+12}	$11.0905^{(i)}$	$12.7562^{(i)}$	$14.4271^{(i)}$

Table A.2. Arrival times for the partial waves in a sloping water-saturated alluvial layer with a fast-speed rock basement [at location $\boldsymbol{x}_2$ ($\gamma_2 = 90^{\circ}$)].

Partial wave	$\tau_{\pm lp}$	$\tau_{\pm ls}$	τ_M
ϕ_{+1}	$2.2731^{(i)}$	$3.1659^{(i)}$	$5.0975^{(i)}$
ϕ_{+2}	$3.2168^{(i)}$	$4.0368^{(i)}$	$5.3767^{(i)}$
ϕ_{-2}	$3.2168^{(i)}$	$4.0368^{(i)}$	$5.3767^{(i)}$
ϕ_{+3}	$4.1224^{(i)}$	$4.8769^{(i)}$	$5.8038^{(i)}$
ϕ_{-3}	$4.1589^{(i)}$	$4.9049^{(i)}$	$5.8038^{(i)}$
ϕ_{+18}	$4.2193^{(i)}$	$6.5429^{(i)}$	$12.4354^{(i)}$
ϕ_{-18}	$4.2193^{(i)}$	$6.5429^{(i)}$	$12.4354^{(i)}$
ϕ_{+4}	$4.9712^{(i)}$	$5.6755^{(i)}$	$6.3376^{(i)}$
ϕ_{-4}	$4.9712^{(i)}$	$5.6755^{(i)}$	$6.3376^{(i)}$
ϕ_{0}			$5.0000^{(d)}$
ϕ_{-1}			$5.0975^{(d)}$
ϕ_{+17}	$5.1208^{(i)}$	$7.3405^{(i)}$	$12.3957^{(i)}$
ϕ_{+5}	$5.7475^{(i)}$	$6.4263^{(i)}$	$6.9393^{(i)}$
ϕ_{-5}	$5.9058^{(i)}$	$6.5307^{(i)}$	$6.9394^{(i)}$
ϕ_{+16}	$5.9391^{(i)}$	$8.0290^{(i)}$	$12.2772^{(i)}$
ϕ_{-16}	$5.9391^{(i)}$	$8.0290^{(i)}$	$12.2772^{(i)}$
ϕ_{+6}	$6.4379^{(i)}$	$7.1239^{(i)}$	$7.5769^{(i)}$
ϕ_{-6}	$6.4379^{(i)}$	$7.1239^{(i)}$	$7.5769^{(i)}$
ϕ_{+15}	$6.6501^{(i)}$	$8.5888^{(i)}$	$12.0811^{(i)}$
ϕ_{-17}	$6.8408^{(i)}$	$8.8272^{(i)}$	$12.3957^{(i)}$
ϕ_{+7}	$7.0279^{(i)}$	$7.7585^{(i)}$	$8.2249^{(i)}$
ϕ_{+14}	$7.2333^{(i)}$	$9.0045^{(i)}$	$11.8099^{(i)}$
ϕ_{-14}	$7.2333^{(i)}$	$9.0045^{(i)}$	$11.8099^{(i)}$
ϕ_{-7}	$7.3617^{(i)}$	$7.9603^{(i)}$	$8.2250^{(i)}$
ϕ_{+8}	$7.5018^{(i)}$	$8.3147^{(i)}$	$8.8636^{(i)}$
ϕ_{-8}	$7.5018^{(i)}$	$8.3147^{(i)}$	$8.8636^{(i)}$
ϕ_{+13}	$7.6725^{(i)}$	$9.2662^{(i)}$	$11.4666^{(i)}$
ϕ_{+9}	$7.8437^{(i)}$	$8.7727^{(i)}$	$9.4773^{(i)}$
ϕ_{+12}	$7.9562^{(i)}$	$9.3694^{(i)}$	$11.0557^{(i)}$
ϕ_{-12}	$7.9562^{(i)}$	$9.3694^{(i)}$	$11.0557^{(i)}$
ϕ_{+10}	$8.0394^{(i)}$	$9.1123^{(i)}$	$10.0536^{(i)}$
ϕ_{-10}	$8.0394^{(i)}$	$9.1123^{(i)}$	$10.0536^{(i)}$
ϕ_{+11}	$8.0787^{(i)}$	$9.3156^{(i)}$	$10.5824^{(i)}$
ϕ_{-15}	$8.1360^{(i)}$	$9.8042^{(i)}$	$12.0812^{(i)}$
ϕ_{-9}	$8.4159^{(i)}$	$9.1342^{(i)}$	$9.4773^{(i)}$
ϕ_{-13}	$8.8607^{(i)}$	$10.1721^{(i)}$	$11.4667^{(i)}$
ϕ_{-11}	$8.9473^{(i)}$	$9.9210^{(i)}$	$10.5825^{(i)}$

Table A.3. Arrival times for the partial waves in a sloping water-saturated alluvial layer with a fast-speed rock basement [at location x_3, ($\gamma_3 = 180^o$)].

Partial wave	$\tau_{\pm lp}$	$\tau_{\pm ls}$	τ_M
ϕ_{+1}	$1.8511^{(d)}$	$2.7768^{(d)}$	$5.0307^{(d)}$
ϕ_{+2}	$1.9681^{(i)}$	$2.8890^{(d)}$	$5.0650^{(d)}$
ϕ_{+3}	$2.0851^{(i)}$	$3.0055^{(d)}$	$5.1205^{(d)}$
ϕ_{+4}	$2.1987^{(i)}$	$3.1228^{(i)}$	$5.1948^{(d)}$
ϕ_{+18}	$2.2044^{(i)}$	$3.3898^{(i)}$	$6.3668^{(i)}$
ϕ_{-18}	$2.2044^{(i)}$	$3.3898^{(i)}$	$6.3668^{(i)}$
ϕ_{+5}	$2.3054^{(i)}$	$3.2374^{(i)}$	$5.2851^{(d)}$
ϕ_{+17}	$2.3106^{(i)}$	$3.4834^{(i)}$	$6.3576^{(i)}$
ϕ_{+6}	$2.4019^{(i)}$	$3.3456^{(i)}$	$5.3877^{(d)}$
ϕ_{+16}	$2.4066^{(i)}$	$3.5633^{(i)}$	$6.3304^{(i)}$
ϕ_{+7}	$2.4853^{(i)}$	$3.4443^{(i)}$	$5.4991^{(d)}$
ϕ_{+15}	$2.4892^{(i)}$	$3.6269^{(i)}$	$6.2855^{(i)}$
ϕ_{+8}	$2.5531^{(i)}$	$3.5305^{(i)}$	$5.6153^{(i)}$
ϕ_{+14}	$2.5562^{(i)}$	$3.6725^{(i)}$	$6.2242^{(i)}$
ϕ_{+9}	$2.6033^{(i)}$	$3.6014^{(i)}$	$5.7327^{(i)}$
ϕ_{+13}	$2.6053^{(i)}$	$3.6986^{(i)}$	$6.1478^{(i)}$
ϕ_{+10}	$2.6342^{(i)}$	$3.6551^{(i)}$	$5.8477^{(i)}$
ϕ_{+12}	$2.6352^{(i)}$	$3.7044^{(i)}$	$6.0580^{(i)}$
ϕ_{+11}	$2.6449^{(i)}$	$3.6897^{(i)}$	$5.9572^{(i)}$
ϕ_{-2}	$2.7486^{(d)}$	$3.5676^{(d)}$	$5.0650^{(d)}$
ϕ_{-3}	$2.8656^{(i)}$	$3.6798^{(d)}$	$5.1205^{(d)}$
ϕ_{-4}	$2.9827^{(i)}$	$3.7963^{(d)}$	$5.1948^{(d)}$
ϕ_{-5}	$3.0962^{(i)}$	$3.9136^{(i)}$	$5.2851^{(d)}$
ϕ_{-6}	$3.2029^{(i)}$	$4.0282^{(i)}$	$5.3877^{(d)}$
ϕ_{-7}	$3.2994^{(i)}$	$4.1364^{(i)}$	$5.4991^{(d)}$
ϕ_{-17}	$3.3041^{(i)}$	$4.3540^{(i)}$	$6.3576^{(i)}$
ϕ_{-8}	$3.3829^{(i)}$	$4.2351^{(i)}$	$5.6153^{(d)}$
ϕ_{-16}	$3.3868^{(i)}$	$4.4177^{(i)}$	$6.3304^{(i)}$
ϕ_{-9}	$3.4507^{(i)}$	$4.3213^{(i)}$	$5.7327^{(i)}$
ϕ_{-15}	$3.4537^{(i)}$	$4.4633^{(i)}$	$6.2856^{(i)}$
ϕ_{-10}	$3.5008^{(i)}$	$4.3922^{(i)}$	$5.8477^{(i)}$
ϕ_{-14}	$3.5029^{(i)}$	$4.4894^{(i)}$	$6.2242^{(i)}$
ϕ_{-11}	$3.5317^{(i)}$	$4.4459^{(i)}$	$5.9572^{(i)}$
ϕ_{-13}	$3.5328^{(i)}$	$4.4952^{(i)}$	$6.1478^{(i)}$
ϕ_{-12}	$3.5425^{(i)}$	$4.4805^{(i)}$	$6.0580^{(i)}$
ϕ_0			$5.0191^{(d)}$
ϕ_{-1}			$5.0307^{(d)}$